Paths from weak to strong coupling in NMR

S. Appelt,[1,*] F. W. Häsing,[1] U. Sieling,[1] A. Gordji-Nejad,[1] S. Glöggler,[2] and B. Blümich[2]
[1]*Central Institute for Electronics, Research Center Jülich, D-52425 Jülich, Germany*
[2]*Institute for Technical Chemistry and Macromolecular Chemistry, RWTH Aachen, D-52056 Aachen, Germany*
(Received 4 November 2009; published 23 February 2010)

J-coupled nuclear magnetic resonance (NMR) spectroscopy in the strong coupling regime at low magnetic field (10^{-7} T $< B < 10^{-3}$ T) is more complex than at high field ($B > 10^{-3}$ T) and at ultralow field ($B < 10^{-7}$ T). We show that several upper and lower boundaries B_i^{up} and B_i^{low} of the magnetic field B exist, where the complexity of *J*-coupled NMR spectra changes in terms of the number of lines. The index $i = 1, 2, \ldots$ for B_i^{up} at high field specifies the perturbation order of the dominating Zeeman interaction and for B_i^{low} at ultralow field the perturbation order of the dominating *J*-coupling interaction. Mathematical expressions for these boundaries are derived for the case of a *J*-coupled S-I_N group where S and I are rare and abundant spins $\frac{1}{2}$ and N counts the abundant spins I. The entire B-field range can further be delineated into two weak coupling regimes, one at high field with $B_2^{\mathrm{up}} < B < B_1^{\mathrm{up}}$ (10^{-3} T $< B < 10^{2}$ T), one at low field with $B_1^{\mathrm{low}} < B < B_2^{\mathrm{low}}$($10^{-8}$ T $< B < 10^{-7}$ T), and a strong coupling regime with $B_2^{\mathrm{low}} < B < B_2^{\mathrm{up}}$ (10^{-7} T $< B < 10^{-3}$ T). The corresponding NMR spectra for the S-I_N group are investigated by experiment and by simulation. In the strong coupling regime, the maximum number of lines is $(N+1)^2$. In the weak coupling regime $B_1^{\mathrm{low}} < B < B_2^{\mathrm{low}}$ at low field, symmetric multiplet structures group around the frequencies 0, J, $(3/2)J$, $2J$, $(5/2)J$, etc. These spectra determine the structure of the S-I_N group unambiguously and are in dual correspondence to the weakly coupled spectra at high field. High-resolution NMR spectroscopy at ultralow field may open up new ways for chemical analysis by small and mobile instruments with many applications in science and technology.

DOI: 10.1103/PhysRevA.81.023420 PACS number(s): 33.25.+k, 32.30.Dx, 82.56.−b

I. INTRODUCTION

Nuclear magnetic resonance (NMR) spectroscopy and magnetic resonance imaging (MRI) at high field are indispensable analytical tools for many areas in science, medicine, and technology [1–7]. High-field NMR spectra have a simple structure because all spin interaction energies (the chemical shift, the direct, and the indirect spin-spin interactions [3–5]) are small compared to the large Zeeman energies so that first-order perturbation theory is sufficient to describe the NMR spectrum with high accuracy. At zero field, the NMR spectrum is again simple. In the last decades, zero-field NMR and nuclear quadrupole resonance (NQR) had their impact in fundamental research and materials science [8–13]. Recent developments in portable ex situ and in situ high-resolution NMR spectroscopy in the 0.1 T regime [14,15] and studies of high-resolution *J*-coupled spectroscopy at field strengths between Earth's field and zero field [16–23] provide new alternatives to high-field NMR spectroscopy with portable and inexpensive devices. One important phenomenon associated with NMR at low field is the strong coupling regime [22,23], which is the range of magnetic fields where the nuclear Zeeman energies are comparable to the energies of the interactions between the spins. Little is known about an exact delineation [1–7] of the strong coupling regime. In this contribution we investigate these boundaries and analyze the complexity of the *J*-coupled spectra at and in between these boundaries. A dual correspondence between NMR spectra at high field and the corresponding spectra close to zero field is demonstrated. In Sec. II, the boundaries are derived by example of the S-I_3 group as a special case of the chemical group S-I_N where one rare spin S couples to N abundant spins I via the heteronuclear J coupling. The strong coupling regime is defined in terms of the *J*-coupling strength, the line width, and the Larmor frequencies. Sec. III provides measured evidence in support of this theory in the low-field regime. Spectra in the ultralow-field regime could not be measured with the available instrumentation. They are simulated and their selection rules discussed in Sec. IV. From the analysis of the *J*-coupled spectra at ultralow field the question arises whether or not a magnetic field is needed at all in order to characterize the chemical structure of molecules by NMR. The appendix gives the calculation of the transitions frequencies for the S-I_N spin system with arbitrary N and derives the maximum number of observable lines as $(N+1)^2$.

II. THEORY

A. General considerations

In the following we will discuss the structure of the *J*-coupled NMR spectra from high field down to zero field and explore the values of the magnetic field where the NMR spectrum changes its structure in terms of the number of observable lines. Consider the S-I_N group [Fig. 1(a)] where a rare spin $S = 1/2$ with angular momentum operator $\vec{S}$ is J coupled to N spins $I = 1/2$ with angular momentum operators $\vec{I}_k (k = 1, 2, \ldots N)$. Assuming that all spins interact with a magnetic field B pointing along the z direction and that J is the heteronuclear *J*-coupling constant we can write the Hamilton operator as

$$H = \underbrace{\omega_S S_z + \omega_I \sum_{k=1}^{N} I_{kz}}_{H^{\mathrm{z}}} + \underbrace{2\pi J \vec{S} \cdot \sum_{k=1}^{N} \vec{I}_k}_{H^{\mathrm{het}}}, \qquad (1)$$

*st.appelt@fz-juelich.de

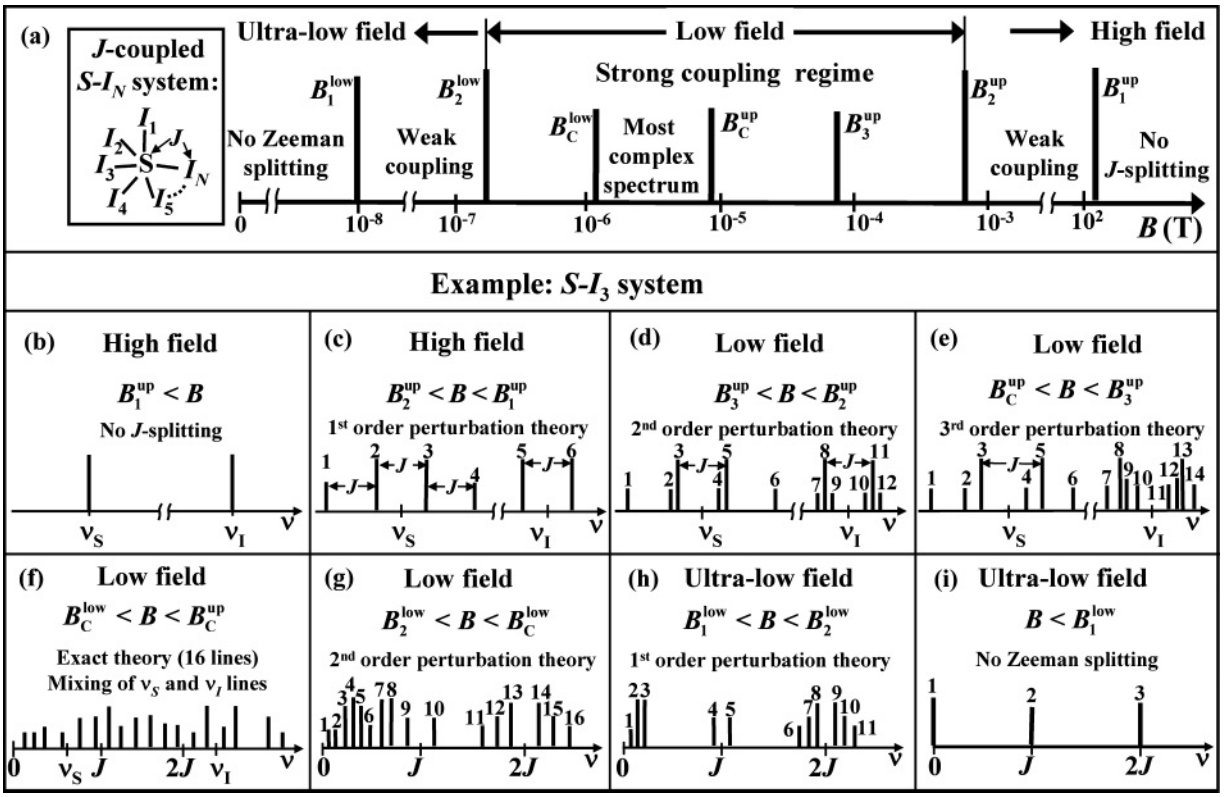

FIG. 1. (a) Strong and weak coupling regimes of the S-I_N system as a function of magnetic field B. (b–i) Stick spectra of the J-coupled S-I_3 system at different field regimes. (b) Stick spectrum at very high field, $B > B_1^{\mathrm{up}}$, (c) in the weak coupling regime at high field, $B_2^{\mathrm{up}} < B < B_1^{\mathrm{up}}$, (d–g) in the strong coupling regime $B_2^{\mathrm{low}} < B < B_2^{\mathrm{up}}$, (h) in the weak coupling regime at low field, $B_1^{\mathrm{low}} < B < B_2^{\mathrm{low}}$, and (i) close to zero field, $B < B_1^{\mathrm{low}}$. See text for details.

where $\omega_I = 2\pi\nu_I = 2\pi\gamma_I B$ and $\omega_S = 2\pi\nu_S = 2\pi\gamma_S B$ are the angular Larmor frequencies of the spins I and S corresponding to the Larmor frequencies ν_I and ν_S. γ_I and γ_S are the gyromagnetic ratios of I and S. H^Z represents the Zeeman interaction of both spin species I and S with the magnetic field B, and H^{het} is the Hamilton operator of the heteronuclear J coupling.

We derive here a mathematical model for several strong and weak coupling regimes that are separated by several upper boundaries B_i^{up} and lower boundaries B_i^{low}, $i \in \mathbb{N}$, as indicated in Fig. 1(a). The index i is associated with the order of perturbation theory used to evaluate the transition frequencies of Eq. (1). Perturbation theory can be applied for $H^{\mathrm{het}} \ll H^z$ at high field and vice versa at low field. The calculation of the transition frequencies of the S-I_N system for arbitrary N is shown in Appendix A.

B. Boundaries between the weak and the strong coupling regime for the S-I_3 group

For clarity we discuss in the following as a representative example the evolution of the J-coupled S-I_3 spectrum over the entire B-field regime and explain the underlying physics of these spectra in the following sections. We assume that B is not perfectly homogeneous, so the line width $\Delta\nu$ is broadened at very high field due to dephasing in an inhomogeneous field. Assuming $J = 100$ Hz and a magnetic field inhomogeneity of 25 ppb, the ^{1}H line is broadened to 100 Hz if $B = 100$ T. Thus, for $B > B_1^{\mathrm{up}} = 100$ T, a splitting due to the J coupling is not observable since $\Delta\nu > J$ and only two lines at frequencies ν_I and ν_S can be observed, as indicated in Fig. 1(b). So B_1^{up} is a boundary dominated by the field inhomogeneity and by the chosen pulse sequence.

In the field range $B_2^{\mathrm{up}} < B < B_1^{\mathrm{up}}$ we enter the weak coupling regime in high field, $\Delta\nu < J$ is valid, and first-order perturbation theory leads to the well-known multiplet splitting. For example, the J-coupled spectrum of the S-I_3 group is an I-spin doublet and an S-spin quartet. For $B_2^{\mathrm{low}} < B < B_2^{\mathrm{up}}$ (low-field regime) the strong coupling regime is entered [Figs. 1(d)–1(g)] and second- and higher-order perturbation theory leads to several line splittings of the NMR spectrum, resulting into more and more complicate multiline spectra. Inside the strong coupling regime eventually higher-order boundaries B_i^{up}, $i \geqslant 3$ exist, as indicated in Figs. 1(a) and 1(e). For $B_C^{\mathrm{low}} < B < B_C^{\mathrm{up}}$ the spectrum has its most complex form [Fig. 1(f)] and a maximum number of lines can be observed. For $B < B_C^{\mathrm{up}}$ the group of I transitions starts to overlap with the group of the S transitions.

On the other side when starting from $B = 0$ [Fig. 1(i)], the spectrum is simple and is characterized by only a few lines (here three). This simple spectrum reflects the internal molecular fields that are responsible for the J coupling but contains no information about the spin species. The spectrum of Fig. 1(i) can be seen as the dual correspondent to the spectrum of Fig. 1(b). The simple structure of Fig. 1(i) holds as long as $B < B_1^{\mathrm{low}}$. B_1^{low} is roughly the boundary where

the Zeeman splitting starts to be larger than the line width $\Delta\nu$. For $B_1^{\text{low}} < B < B_2^{\text{low}}$ the weak coupling regime at low field is entered. Here, first-order perturbation theory leads to a splitting of each line in Fig. 1(i) into a characteristic number of lines, in our case into 11 lines [Fig. 1(h)]. This spectrum with three groups at frequency zero, J, and 2 J fully characterizes the molecular structure and can be viewed as the dual correspondent of the weak coupled spectrum in Fig. 1(c). As will be shown later both B_1^{low} and B_2^{low} are boundaries that depend on the line width, the J-coupling constant, and the gyromagnetic ratios. The line width in ultralow field is dominated by the T_2 relaxation time and not by field inhomogeneity. For $B > B_2^{\text{low}}$, the strong coupling regime is entered from the low-field side and second- and higher-order perturbation theory leads to an increasing line splitting until the maximum number of lines (here 16) is reached [Fig. 1(g)]. For $B > B_C^{\text{low}}$ [Fig. 1(f)], the group of lines at zero frequency starts to overlap with the group of lines at frequency J.

In the following the corresponding mathematical expressions for these boundaries B_i^{up} and B_i^{low} are derived, the spectra below and above B_i^{up} and B_i^{low} are analyzed, and the maximum number of lines is accounted for. The transition frequencies of the S-I_N group in high and in low field can be extracted from the eigenvalues obtained by diagonalization of the Hamilton operator Eq. (1), then expanding the eigenvalues in a Taylor series up to the second order and by applying the selection rules in high or in low field. This procedure is shown in Appendices A and B. Without losing generality, we restrict in the following to the S-I_3 group. In high field we have $|\nu_I - \nu_S| \gg J$ and from the Taylor series in the parameter $J/(\nu_I - \nu_S)$ and the selection rules in high field (see Appendix A) we obtain six transitions of the S spin near ν_S:

$$\nu_1 = \nu_S - \tfrac{3}{2}J - \tfrac{3}{4}J^2/(\nu_I - \nu_S) \tag{2}$$

$$\nu_{2,4} = \nu_S \mp \tfrac{1}{2}J - \tfrac{7}{4}J^2/(\nu_I - \nu_S) \tag{3}$$

$$\nu_{3,5} = \nu_S \mp \tfrac{1}{2}J - \tfrac{1}{4}J^2/(\nu_I - \nu_S) \tag{4}$$

$$\nu_6 = \nu_S + \tfrac{3}{2}J - \tfrac{3}{4}J^2/(\nu_I - \nu_S), \tag{5}$$

and six transitions of the I spin near ν_I:

$$\nu_{7,10} = \nu_I \mp \tfrac{1}{2}J - \tfrac{1}{4}J^2/(\nu_I - \nu_S) \tag{6}$$

$$\nu_{8,11} = \nu_I \mp \tfrac{1}{2}J + \tfrac{1}{4}J^2/(\nu_I - \nu_S) \tag{7}$$

$$\nu_{9,12} = \nu_I \mp \tfrac{1}{2}J + \tfrac{3}{4}J^2/(\nu_I - \nu_S). \tag{8}$$

These transitions are illustrated in Fig. 1(d). The spectrum of the S-I_3 group in high field [Fig. 1(c)] reflects the well-known J-coupled doublet at frequencies $\nu_I \pm \frac{1}{2}J$ and the quartet at frequencies $\nu_S \pm \frac{3}{2}J$ and $\nu_S \pm \frac{1}{2}J$. This first-order line splitting is observable if $\Delta\nu < J$. Therefore, coming from high field, B_1^{up} is the magnetic field strength at which the J-coupling structure appears for the first time.

The doublet and quartet structure is maintained down to $B = B_2^{\text{up}}$. Below B_2^{up} the I-spin spectrum starts to split into a pair of three lines [Fig. 1(d)]. According to Eqs. (6)–(8) the line splitting between these three lines is $J^2/[2(\nu_I - \nu_S)]$. Thus we can define the upper boundary B_2^{up} by the requirement that the splitting starts to be observable if $\Delta\nu < J^2/[2(\nu_I - \nu_S)]$. So the upper boundary B_2^{up} is given by

$$B_2^{\text{up}} = J^2/[2\Delta\nu(\gamma_I - \gamma_S)]. \tag{9}$$

An inspection of the S-I_N transition frequencies for $N \neq 3$ shows that for the I spin B_2^{up} is valid independent of N (see Appendix A). This is not so for the S spin [27] where according to Eqs. (3) and (4) the splitting is given by $3J^2/[2(\nu_I - \nu_S)]$. In a similar way we can define B_3^{up} by inspection of third-order perturbation theory (not shown here). As a result, for $\Delta\nu < 3J^3/4(\nu_I - \nu_S)^2$, a further splitting occurs as shown in Fig. 1(e). Thus the high-field boundary to third order is

$$B_3^{\text{up}} = \sqrt{3J^3/[4\Delta\nu(\gamma_I - \gamma_S)^2]}. \tag{10}$$

From Eqs. (5) and (6) the field B_C^{up} where the group of I transitions start to overlap with the group of S transitions can be derived as $B_C^{\text{up}} = (1 + 1/\sqrt{2})J/(\gamma_I - \gamma_S)$.

In order to derive the lower boundaries B_i^{low}, we need to calculate the transition frequencies by applying perturbation theory close to zero field, where $J \gg (\nu_I - \nu_S)$ is valid. The procedure for arbitrary N is shown in Appendix B. Expanding the exact transition frequencies into a Taylor series up to the second order in the parameter $(\nu_I - \nu_S)/J$, we obtain for the S-I_3 group 16 transition frequencies. These transitions are arranged into three groups [Fig. 1(g)]. The first group consists of eight transitions close to zero frequency, which we define as the zero-frequency transitions (0 transitions):

$$\nu_{1,2} = \frac{1}{2}(\nu_I + \nu_S) \mp \frac{(\nu_I - \nu_S)^2}{4J} \tag{11}$$

$$\nu_{3,6} = \frac{1}{4}(3\nu_I + \nu_S) \mp \frac{3(\nu_I - \nu_S)^2}{32J} \tag{12}$$

$$\nu_{4,5} = \frac{1}{4}(3\nu_I + \nu_S) \mp \frac{(\nu_I - \nu_S)^2}{32J} \tag{13}$$

$$\nu_{7,8} = \frac{1}{4}(5\nu_I - \nu_S) \mp \frac{(\nu_I - \nu_S)^2}{32J}. \tag{14}$$

The second group consists of two transitions centered near the frequency J, which we call the J transitions:

$$\nu_{9,10} = J \mp \frac{1}{2}(\nu_I + \nu_S) \pm \frac{(\nu_I - \nu_S)^2}{4J}. \tag{15}$$

The third group consists of six transitions near frequency $2J$:

$$\nu_{11,16} = 2J \mp \frac{1}{4}(5\nu_I - \nu_S) + \frac{7(\nu_I - \nu_S)^2}{32J} \tag{16}$$

$$\nu_{12,15} = 2J \mp \frac{1}{4}(3\nu_I + \nu_S) + \frac{7(\nu_I - \nu_S)^2}{32J} \tag{17}$$

$$\nu_{13,14} = 2J \mp \frac{1}{4}(\nu_I + 3\nu_S) + \frac{3(\nu_I - \nu_S)^2}{32J}. \tag{18}$$

At $B = 0$ the spectrum predicted by Eqs. (11)–(18) reduces to three lines at frequencies 0, J, and 2 J [Fig. 1(i)]. For $B_1^{\text{low}} < B < B_2^{\text{low}}$ we have $\nu_I - \nu_S \ll J$ so the second-order terms proportional to $(\nu_I - \nu_S)^2$ in Eqs. (11)–(18) can be neglected and 11 first-order transitions remain. These 11 transitions [Fig. 1(h)] are identified as three zero-frequency transitions at $\nu_1 = \frac{1}{2}(\nu_I + \nu_S)$, $\nu_2 = \frac{1}{4}(3\nu_I + \nu_S)$, and $\nu_3 = \frac{1}{4}(5\nu_I - \nu_S)$, two J transitions, and six 2 J transitions. Their frequencies result from linear combinations of γ_I and γ_S. The coefficients

of these linear combinations define new total gyromagnetic ratios, which reflects the relative spin orientation of all coupled spins. The general form of these linear combinations for arbitrary N is shown in Appendix B. Note if $\gamma_I \to \gamma_S$ all the J and 2 J transitions Eqs. (15)–(18) vanish because homonuclear J couplings between magnetically equivalent spins cannot be observed [6]. Furthermore, all three 0 transitions, ν_1–ν_3, collapse to the trivial case of one observable line at frequency $\nu_0 = \gamma_I B$.

The first lower boundary B_1^{low} starting from zero is the field B from where the first splitting is observable. From Eqs. (11) to (18) we see that the largest splitting is given by Eq. (15). It is observable if $\Delta\nu < (\gamma_I + \gamma_S)\, B$. Therefore B_1^{low} is given by

$$B_1^{\text{low}} = \Delta\nu/(\gamma_I + \gamma_S). \tag{19}$$

We can show that Eq. (19) is valid for $N = 1, 3$ but for $N = 2, 4$ Eq. (19) is modified by $B_1^{\text{low}} = 3\Delta\nu/[2(\gamma_I - \gamma_S)]$ (see Appendix B). The next lower boundary B_2^{low} can be found from Eqs. (11)–(18) by identifying the largest line splitting, which is proportional to $(\nu_I - \nu_S)^2$. The J and 2 J lines do not split further but the three zero transitions at $B_1^{\text{low}} < B < B_2^{\text{low}}$ split successively into eight lines once $B > B_2^{\text{low}}$. The largest splitting given by Eq. (11) is $(\nu_I - \nu_S)^2/2J$ so B_2^{low} can be derived from the condition $\Delta\nu < (\nu_I - \nu_S)^2/2J$, giving

$$B_2^{\text{low}} = \sqrt{\frac{2\Delta\nu J}{(\gamma_I - \gamma_S)^2}}. \tag{20}$$

We found that no further lower boundary B_3^{low} exists that would increase the number of lines, so for $B > B_2^{\text{low}}$ the maximum number of 16 lines is reached. From Eqs. (14) and (15) the field B_C^{low} where the 0 transitions start to overlap with the J transitions can be estimated as $B_C^{\text{low}} \approx 4J/(7\gamma_I + \gamma_S)$.

In summary the strong coupling regime $B_2^{\text{low}} < B < B_2^{\text{up}}$ for the S-I_3 group in terms of the field B is given by

$$\sqrt{\frac{2\Delta\nu J}{(\gamma_I - \gamma_S)^2}} < B < \frac{J^2}{2\Delta\nu\,(\gamma_I - \gamma_S)}. \tag{21}$$

We can express Eq. (21) in an elegant way by introducing the dimensionless parameter $(\nu_I - \nu_S)/J$. From the two conditions for the strong coupling boundary, $\Delta\nu < J^2/2\,(\nu_I - \nu_S)$ for B_2^{up} and $\Delta\nu < (\nu_I - \nu_S)^2/2J$ for B_2^{low}, we see that the strong coupling regime in the parameter $(\nu_I - \nu_S)/J$ is

$$\frac{2\Delta\nu}{\nu_I - \nu_S} < \frac{\nu_I - \nu_S}{J} < \frac{J}{2\Delta\nu}. \tag{22}$$

One can show that the right side of Eq. (22) is valid independent of N, while the left side of Eq. (22) holds for odd N but has to be multiplied by a factor 1/2 for even N (see Appendices A and B). The dual correspondence of the two weak coupling regimes at high ($B_2^{\text{up}} < B < B_1^{\text{up}}$) and low field ($B_1^{\text{low}} < B < B_2^{\text{low}}$) has the following meaning: For $B_2^{\text{up}} < B < B_1^{\text{up}}$ the dominant Zeeman interaction defines the nuclear spin species and the J coupling is a small perturbation whose characteristic splitting defines the internal molecular fields and the number of coupled spins. For $B_1^{\text{low}} < B < B_2^{\text{low}}$ the dominant interaction is the J coupling, which is a measure of the internal field, and the small perturbation is the Zeeman interaction whose characteristic splitting defines the nuclear spin species and the number of coupled spins.

III. EXPERIMENTAL VERIFICATION OF THE UPPER BOUNDARIES

Typical numerical values for B_i^{up} and B_i^{low} can be calculated from the theory if we assume J-coupled NMR spectroscopy of a $^{13}CH_3$ group with $\gamma_H = 42.57$ MHz/T, $\gamma_C = 10.78$ MHz/T and by choosing $^1J_{H,C} = 140$ Hz and $\Delta\nu = 0.33$ Hz. From Eqs. (9), (10), (19), and (20) we get $B_2^{\text{up}} = 10^{-3}$ T, $B_3^{\text{up}} = 8.3 \times 10^{-5}$ T, $B_1^{\text{low}} = 6.2 \times 10^{-9}$ T, and $B_2^{\text{low}} = 3 \times 10^{-7}$ T. In order to test the upper boundaries B_2^{up} and B_3^{up} experimentally we built a low-field NMR spectrometer [see Fig. 2(a)] that measures high-resolution NMR spectra at nuclear Larmor frequencies ranging 5–250 kHz. We improved the low-field NMR setup as described in Ref. [22] to gain higher signal-to-noise ratio and higher spectral resolution. The signal-to-noise ratio is improved by prepolarizing the sample in a 2-T Halbach magnet and by employing a radio frequency shield, which surrounds the receiver coil and the preamplifier [16,39]. The spectral resolution is improved to reach the ppm range by using a two-coil electromagnet (60-cm diameter), which produces a magnetic field B in the range 2×10^{-4} T $< B < 5 \times 10^{-3}$ T with a homogeneity of about 1 ppm/cm^3. For measurements in Earth's field (5×10^{-5} T) we used a high-resolution Earth's field NMR spectrometer [Fig. 2(a), left] [19,22]; 0.2 cm^3 of 99% ^{13}C-enriched methanol (HO-$^{13}CH_3$) is used as an example for the S-I_3 group. The labile OH proton is not involved into the J-coupled network and therefore gives rise to a free proton line at the Larmor frequency $\nu_0 = \gamma_H B$. ^{13}C NMR signals down to 41 kHz Larmor frequency (3.92×10^{-3} T) can be measured in a single scan. This is demonstrated in the inset of Fig. 2(b), which shows the free induction decay (FID) of ^{13}C nuclei from methanol. The corresponding ^{13}C spectrum in Fig. 2(b) shows a quartet structure with a line separation of $^1J_{H,C} = 140.5$ Hz. The corresponding ^{1}H FID measured at 167 kHz is shown in the inset of Fig. 2(c). The ^{1}H spectrum shows a doublet split by $^1J_{H,C}$ and the free proton line of the OH group, which is located in the center between the two doublet lines. The form of both spectra is exactly what is expected from high-field NMR except in high field (say at 500 MHz) the position of the OH line would be shifted by about 750 Hz from the central position of the $^{13}CH_3$ doublet due to the chemical shift difference of $|\delta_{OH} - \delta_{CH3}| = 1.5$ ppm.

The high-field boundaries B_2^{up} and B_3^{up} can be proved experimentally by measuring J-coupled NMR spectra at different fields. Figures 3(a)–3(d) show four ^{1}H methanol ($^{13}CH_3$-OH) spectra measured at $B = 3.93 \times 10^{-3}$ T, 9.88×10^{-4} T, 2.5×10^{-4} T, and 4.84×10^{-5} T (Earth's field). The lower traces correspond to the measured spectrum and the upper traces to simulations based on the density matrix and product operator formalism [28]. From the spectra we obtain $^1J_{H,C} = 140.5$ Hz and the experimental line widths of $\Delta\nu = 0.83$ Hz for Fig. 3(a), $\Delta\nu = 0.32$ Hz for Fig. 3(b) and 3(c), and $\Delta\nu = 0.26$ (0.38) Hz for the singlet (triplet) lines in Fig. 3(d). Neither ^{1}H doublet line in Fig. 3(a) is split. But at 9.88×10^{-4} T [Fig. 3(b)] each doublet line starts to split into three lines. This is expected according to Eq. (9), which predicts a splitting into three lines below $B_2^{\text{up}} = 10^{-3}$ T.

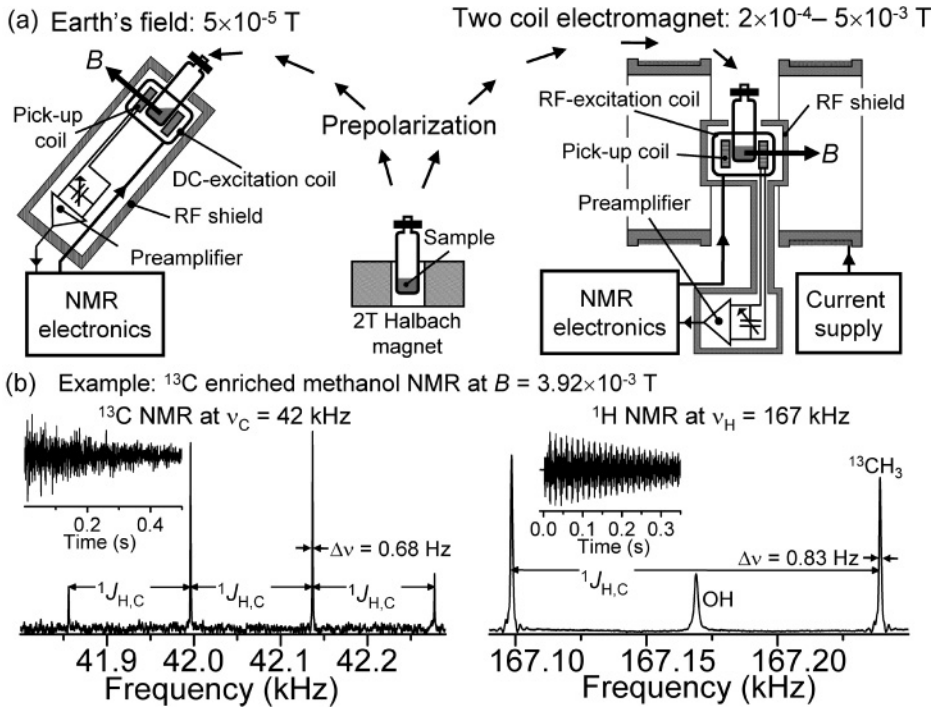

FIG. 2. Experimental setup. (a) Earth's field NMR (left) and low-field NMR (right). The liquid sample (0.2 cm^3) is prepolarized by a 2-T Halbach magnet and then placed into the pick-up coil of either NMR spectrometer. The free induction decay (FID) is measured following a 90° pulse excitation. (b) NMR spectroscopy of ^{13}C-enriched methanol at $B = 3.92 \times 10^{-3}$ T. (Left) Single scan FID of ^{13}C (insert) and corresponding ^{13}C spectrum at 42 kHz. (Right) Single scan ^{1}H FID (insert) and corresponding ^{1}H spectrum at 167 kHz. The measured J-coupling constant is $^1J_{H,C} = 140.5$ Hz. The central line corresponds to the OH group at frequency $\nu_H = 167.14$ Hz.

This splitting is more pronounced at lower field [Fig. 3(c)]. At 4.8×10^{-5} T [Fig. 3(d)] each central line of the two triplets in Fig. 3(c) is split further into two lines, which results in a pair of four lines. This splitting is explained by third-order perturbation theory [27] below $B_3^{up} = 8.3 \times 10^{-5}$ T. The pair of four lines can also be explained by the vector model [22,23], which states that one proton of the $^{13}CH_3$ group is observed and the other two protons are strongly coupled to either a singlet or a triplet state. These four states split the single resonance of each doublet line into four lines. All experimental results are in excellent agreement with the simulations and with the predictions for the upper boundaries.

IV. COMPLEXITY OF THE S-I_N GROUP FOR $B < B_2^{up}$

A. S-I_3 spectrum versus magnetic field

As there is good agreement between all experiments and simulations in the range 5×10^{-5} T $< B < 4 \times 10^{-3}$ T we can compare our theoretical predictions with simulations in the field range $0 < B < 10^{-4}$ T. The eight simulated spectra in Fig. 4 of the J-coupled $^{13}CH_3$ group ($^1J_{H,C} = 140.5$ Hz, $\Delta\nu = 0.33$ Hz) show the evolution from a simple spectrum at high field [Fig. 4(a)] to a spectrum with high complexity [Fig. 4(d)] and back to a simple spectrum at zero field [Fig. 4(h)]. For the simulations, the detection operator $I^{det} = \gamma_S S_x + \gamma_I \sum_{k=1}^{N} I_{kx}$ is used. The ^{1}H doublet and ^{13}C quartet of Fig. 4(a) serves as a reference in high field. They agree well with the experimental result in Fig. 2(b). For $B = 10^{-4}$ T [Fig. 4(b)], each doublet line splits into three lines [as in Fig. 3(b)] and for the ^{13}C spectrum six lines are observed. The six ^{13}C lines, as predicted by Eqs. (2)–(5), can also be explained by the vector model, where three strongly coupled protons form either a quartet (total spin 3/2) or a doublet (total spin 1/2) [22]. At 10^{-5} T [Fig. 4(c)] still six ^{13}C lines are visible while the ^{1}H spectrum splits into a pair of four lines. In addition, two further lines appear at frequencies 790 and 900 Hz. Quantum mechanics reveals that the two lines can be explained by a three-quantum process where simultaneously two protons flip down and the carbon nucleus flip up or vice versa, so the total z magnetization changes by ±1. This three-quantum process can occur with the remaining proton spin of the $^{13}CH_3$ group either in the up or down position. The total number of 16 $(8 + 6 + 2)$ transitions in Fig. 1(c) does not increase further when the field is further decreased. So the maximum number of 16 lines is a result of an "extended" vector model with single- and triple-quantum transitions. At 2×10^{-6} T [Fig. 4(d)] the three groups of Fig. 4(c) start to mix. This 16-line spectrum has the highest complexity in the sense that there is no obvious ordering and that perturbation theory does not converge and is not applicable. For $B = 6 \times 10^{-7}$ T, which is above $B_2^{low} = 3 \times 10^{-7}$ T [Fig. 4(e)], the number of lines is reduced from 16 to 12 and these lines group into four transitions close to zero, into two lines near frequency J and into a pair of three lines near frequency 2 J. For $B = 2 \times 10^{-7}$ T [Fig. 4(f)], the weak coupling regime $B_1^{low} < B < B_2^{low}$ applies, and 11 lines appear as expected by the theory. Above the lower boundary $B_1^{low} = 6.2 \times 10^{-9}$ T [Fig. 4(g)], the first splitting appears at J and 2 J. For $B < B_1^{low}$ and at $B = 0$, the spectrum collapses into three lines at frequencies zero, J, and at 2 J [Fig. 4(h)]. The simulated and calculated zero-field spectrum agrees with a recent experimental result published by Ledbetter *et al.* [13], who measured the zero-field spectrum of ^{13}C-enriched methanol by using an atomic magnetometer located inside a magnetic shield. Unfortunately, the zero-field spectrum is not suited to characterize a chemical group in an unambiguous way. In the following this issue is discussed.

B. Physics of S-I_N spectra close to zero field and selection rules

Until now we have no physical model for the observed transitions close to zero field ($0 < B < 10^{-7}$ T) and no

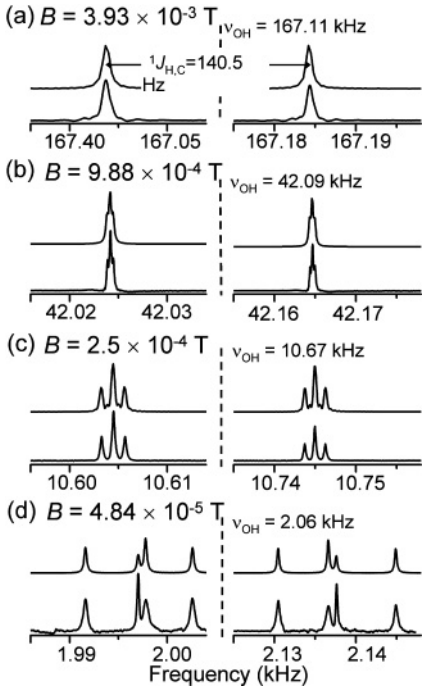

FIG. 3. Comparison between simulated (upper traces) and experimental (lower traces) ^{1}H spectra of 99% ^{13}C-enriched methanol measured at four different frequencies. The central OH line is not shown. The differences in the measured line widths (see text) come from external field fluctuations, fluctuations of the current supply, temperature variations of the sample, and from the field inhomogeneity ($\sim 10^{-6}/\mathrm{cm}^3$) of the electromagnet. The deviations between experiment and simulation in Fig. 3(d) with respect to the signal amplitudes of the two central lines can be explained by a line narrowing (broadening) due to formation of a singlet (triplet) state [22], which is not taken into account for the simulations.

explanation for the maximum number of lines of the S-I_N group. Consider the energy level diagrams of the S-I_N group for $N = 1$–4 (Fig. 5). At $B = 0$, the energy levels of the S-I_N group are given only by the internal molecular fields. The zero-field energies are calculated from diagonalization of H^{het} in Eq. (1) to be $+J/4$ and $-3\ J/4$ for the S-I group, $+J/2$, 0, and $-J$ for the S-I_2 group, $+3J/4$, $J/4$, $-3\ J/4$, and $-5\ J/4$ for the S-I_3 group and $+J$, $J/2$, 0, $-J$, and $-3J/2$ for the S-I_4 group (see Appendix B). Every energy level is associated with a total spin $F = F_S + F_I$. The S spin can assume the two possible values $F_S = \pm 1/2$ with respect to the total I spin with total quantum number $F_I = (N/2) - k$. The number k runs from $k = 0, 1, \ldots N/2$ for even N and $k = 0, 1, \ldots (N-1)/2$ for odd N. For example, the $3\ J/4$, $J/4$, $-3\ J/4$, and $-5\ J/4$ energy level for S-I_3 is associated with a total spin of $F = 2$, 1, 0, and 1, respectively. When a weak magnetic field is applied each total spin state F splits into $2F + 1$ Zeeman levels. As long as $|\nu_I - \nu_S| \ll J$, all transitions inside one F multiplet are equal.

Let us discuss the allowed transitions. Consider the detection operator $I^{\mathrm{det}} = \gamma_S S_x + \gamma_I \sum_{k=1}^{N} I_{kx}$. The selection rules follow by inspection of the transition probabilities $|\langle \Psi_i | I^{\mathrm{det}} | \Psi_j \rangle|^2$, where Ψ_i and Ψ_j are two different eigenfunctions of the Hamiltonian Eq. (1). The possible transitions in Fig. 5 are indicated by solid, dashed, and dotted arrows, which are associated with the 0 transitions, with the J and $3J/2$ transitions and with the $2\ J$ and $5\ J/2$ transitions, respectively. For the zero transitions the following three selection rules are valid: 1) $\Delta F = 0$; 2) $\Delta F_S = 0$; and 3) $\Delta m_F = \pm 1$, where $F_S = \pm 1/2$ and m_F is the total magnetic quantum number along the z direction of the B field. The meaning of this selection rules is that the total spin vector F does not change its length but F changes its orientation such that the z projection of the total angular momentum of the photon ($\pm\hbar$) and the spin system is conserved. The dashed and dotted arrows result from a second set of selection rules: 1) $\Delta F = \pm 1$; 2) $\Delta F_S = \pm 1$; and 3) $\Delta m_F = \pm 1$. For example, for the S-I_3 system the transitions from $F = 2$ ($\mathrm{E} = 3\ J/4$) to $F = 1$ ($\mathrm{E} = J/4$) and from $F = 0$ ($\mathrm{E} = -3\ J/4$) to $F = 1$ ($\mathrm{E} = -5\ J/4$) are forbidden because the second selection rule $\Delta F_S = \pm 1$ is violated. The origin of $\Delta F_S = \pm 1$ is based on the fact that homonuclear J couplings between magnetically equivalent spins cannot be measured [6]. In other words, the radio frequency field cannot change the relative orientations of the I spins but can change the relative orientation between the S and all the other I spins. Note that the flip or flop process of the S spin ($\Delta F_S = \pm 1$) is associated with a sign change in the energies of the two multiplets involved. If $B_1^{\mathrm{low}} < B < B_2^{\mathrm{low}}$ (weak coupling regime) then all zero transitions associated to one multiplet F become degenerate. So the S-I_N system for $N = 1$ has one (ν_1), for $N = 2,3$ three ($\nu_1 - \nu_3$), and for $N = 4$ five different zero transitions ($\nu_1 - \nu_5$). The total number of lines for $N = 1$–4 for $B_1^{\mathrm{low}} < B < B_2^{\mathrm{low}}$ are three, six, 11, and 17, respectively. For $B > B_2^{\mathrm{low}}$ second- and higher-order terms lift the degeneration of the zero transitions inside each F multiplet and the maximum number of lines can be observed. For example, the S-I_3 system has eight possible zero transitions (solid arrows), two J transitions (dashed arrows), and six $2\ J$ transitions (dotted arrows). For $N = 1$–4, the maximum number of lines is four, nine, 16, and 25, respectively. In general, the maximum number of lines for the S-I_N group is $(N+1)^2$. The proof of this statement is given in Appendix C.

The spectra close to zero give rise to the question whether or not we need a magnetic field in order to identify a chemical group in a unique way. Does the zero-field spectrum provide sufficient information to identify the chemical environment of the spins? Consider the left side of Figs. 6(a)–6(e), which shows five simulated zero-field spectra for five different chemical groups ^{13}CH, ^{15}NH$_2$, ^{13}CH$_2$, ^{13}CH$_3$, and ^{13}CH$_4$. Obviously the positions of the lines in the zero-field spectra depend on the strength of $^1J_{\mathrm{H,C}}$ and on the number of coupled spins. This is why in Fig. 6 all (except the zero) line positions in the zero-field ^{13}CH$_N$ spectra are different. Unfortunately the zero-field spectrum cannot be taken as a fingerprint of the molecular structure because it is neither possible to determine the nuclear spin species nor the number of nuclear spins involved. For example, the two zero-field spectra of ^{13}CH and ^{15}NH$_2$ in Figs. 6(a) and 6(b) cannot be distinguished. Both spectra have one line at zero and at 140 Hz because $^1J_{\mathrm{H,C}} \sim 140$ Hz $\neq^1 J_{H,N} \sim 85$–95 Hz but the position of the lines are at $^1J_{\mathrm{H,C}}$ and $3\ ^1J_{H,N}/2$. The situation is different if a small field in the weak coupling regime $B_1^{\mathrm{low}} < B < B_2^{\mathrm{low}}$ is applied. The Zeeman splitting can be used to distinguish the

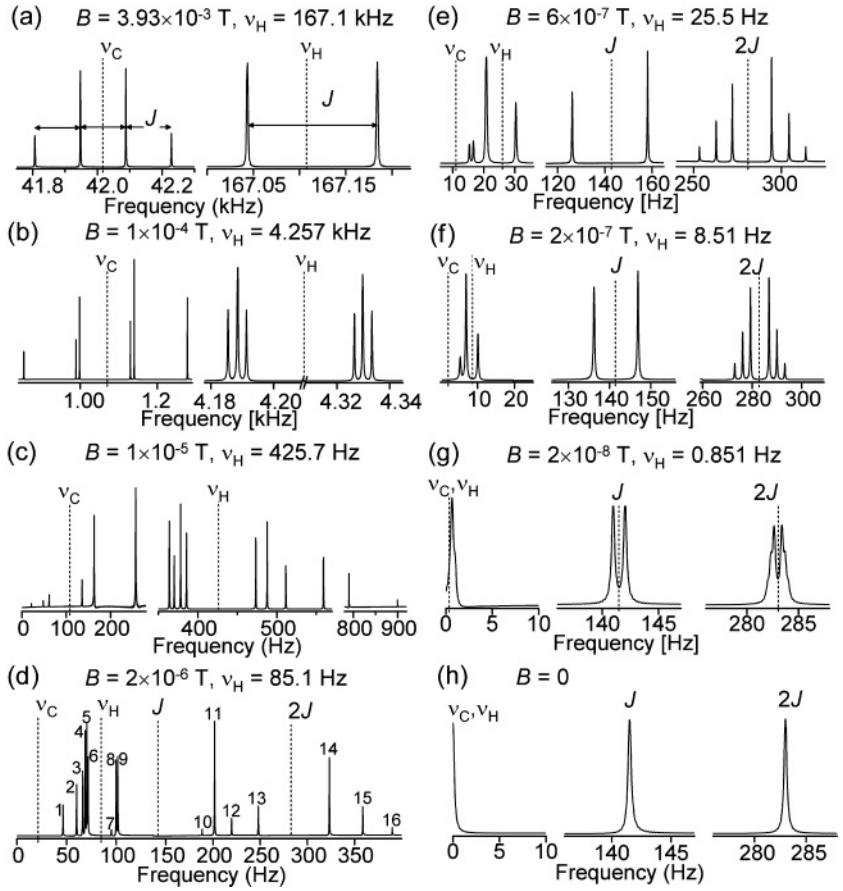

FIG. 4. Simulated spectra of the $^{13}CH_3$ group from high field to zero field. The dotted lines indicate the Larmor frequencies ν_C and ν_H. $J_{H,C} = 140.5$ Hz, and all line widths are $\Delta\nu = 0.33$ Hz. Simulated ^{1}H doublet and ^{13}C quartet at (a) 3.93×10^{-3} T in the weak coupling regime; (b) in the strong coupling regime at 10^{-4} T, where for $B > B_3^{up}$ six ^{13}C lines and a pair of three ^{1}H lines appear; (c) 10^{-5} T ($B < B_3^{up}$), where the ^{1}H spectrum splits into a pair of four lines and two additional combination lines appear; (d) 2×10^{-6} T, where the most complex spectrum with 16 lines can be observed; (e) 6×10^{-7} T, where the spectrum starts to reduce to 12 lines; (f) 2×10^{-7} T (weak coupling regime), where 11 lines are packed in three groups; (g) just above B_1^{low}, where the splitting into 11 lines is still visible, and (h) $B = 0$, where the spectrum reduces to only three lines.

different groups. From the line splitting of the five spectra on the right side of Figs. 6(a)–6(e) we can deduce the number N of I spins and the gyromagnetic ratios of I and S. The number N of coupled I spins is encoded by the number of $2N$ Zeeman lines centered around the frequencies J, $3J/2$, $2J$, and $5J/2$. The gyromagnetic ratios γ_I and γ_S can be calculated explicitly from the zero transitions. For example, from the three zero transitions $\nu_1 = \frac{1}{2}(\nu_H + \nu_C)$, $\nu_2 = \frac{1}{4}(3\nu_H + \nu_C)$, and $\nu_3 = \frac{1}{4}(5\nu_H - \nu_C)$ of the $^{13}CH_3$ group we get $\gamma_H = (\nu_2 + \nu_3)/2B$ and $\gamma_C = (3\nu_1 - 2\nu_2)/B$.

V. CONCLUSION AND OUTLOOK

We presented theoretical and experimental NMR studies of the weak and strong coupling regimes together with their associated upper and lower boundaries for the magnetic field. The NMR spectrum of the S-I_N group for the lower weak coupling regime $B_1^{low} < B < B_2^{low}$ contains sufficient information to determine the structure of the S-I_N group unambiguously. The small field of $\sim 10^{-7}$ T required for the assignment of molecular groups does not need to be homogeneous. In fact a homogeneity of only $\Delta B/B \sim 10^{-3}$

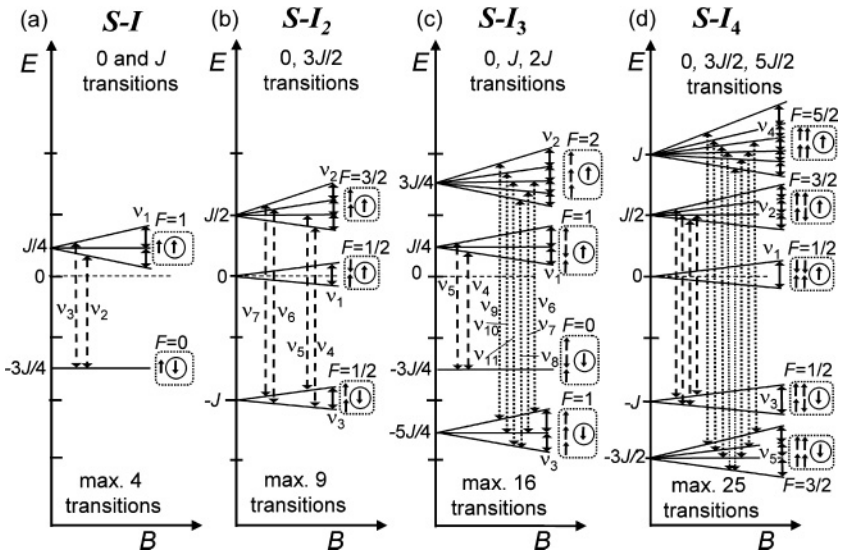

FIG. 5. Energy level diagram of four different S-I_N groups ($N = 1$–4) in ultralow magnetic field ($B < B_2^{low}$). F is the total spin of each energy level. The groups of up and down arrows correspond to the spin configuration of each energy level. The circle around the arrow denotes the S spin. Allowed transitions are indicated by the solid arrows (0 frequency transitions), dashed arrows (J and $3J/2$ transitions) and dotted arrows ($2J$ and $5J/2$ transitions).

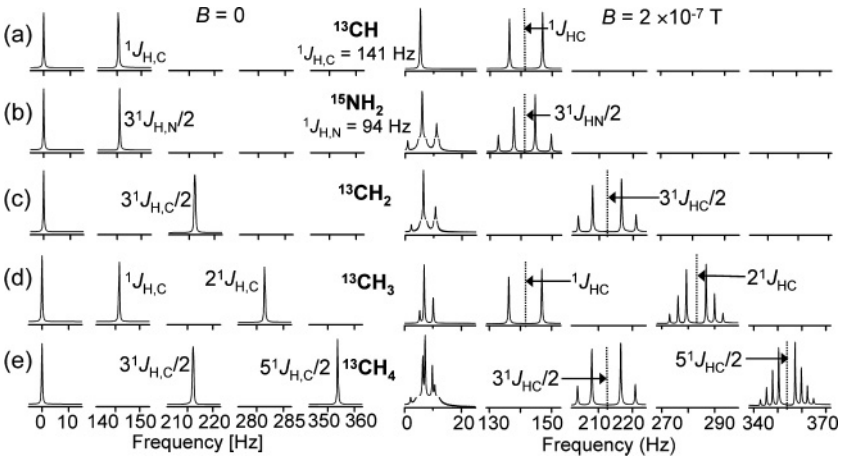

FIG. 6. Simulated *J*-coupled NMR spectra ($\Delta\nu$ =0.33 Hz) near zero field for different molecular groups. (a) ^{13}CH, (b) ^{15}NH$_2$, (c) ^{13}CH$_2$, (d) ^{13}CH$_3$, and (e) ^{13}CH$_4$. Spectra are shown at zero field (left) and in the weak coupling regime at 2×10^{-7} T (right). The two spectra on the left in (a) and (b) do not differ, so the ^{13}CH and ^{15}NH$_2$ group cannot be distinguished at zero field. At 2×10^{-7} T different line splittings arise in the spectra. The number of lines as well as their separations determine the group in a unique way (see text for details).

would produce a ^{1}H line broadening of less than 0.004 Hz, which is absolutely acceptable in high-resolution NMR spectroscopy.

One open question is how to determine structures of large molecules, such as proteins. We found by simulations that the spectrum close to zero field of two and more *J*-coupled molecular groups is very complicate. We do not know yet how to elucidate the molecular structure given these complicate spectra. More theoretical and experimental studies close to zero field need to be done. Another problem is the low signal-to-noise ratio due to the large number of line splittings at low field, especially for large molecules with rare spins in natural abundance. This problem might be solved by a combination of hyperpolarization technologies [29–37] with new sensitive detection methods such as atomic magnetometers [24] or nanosensors on diamond basis [38].

Up to now we have neglected the loss of the chemical shift information at low fields. The chemical shift is a very important additional parameter for multidimensional NMR spectroscopy. Fortunately, it has been found recently, that at low field, small chemical shift differences can be measured even below the resolution limit imposed by the line width [39]. Therefore an intriguing vision for the future is a mobile, low-field, high-resolution NMR spectrometer, the field of which can be scanned and the basic elements of which are a prepolarization unit such as a Halbach magnet or some other hyperpolarizing unit, a low-cost Helmholtz coil, a detector such as a miniaturized atomic magnetometer [13], and a magnetic shield.

Finally we mention that systems like the strongly coupled S-I_N group with a maximum of $(N+1)^2$ lines might be candidates for NMR quantum computing, because the large number of lines comes from rather simple molecular structures that built a network of entangled qubits with long decoherence times. Resuming all facts it is likely that mobile low-field NMR spectroscopy will develop toward a powerful analytical tool and might also play a significant role in the field of quantum information processing.

ACKNOWLEDGMENTS

The authors gratefully acknowledge technical support from G. D'Orsaneo, A. Schwaitzer, and H. Glückler, and financial support from K. Ziemons of the Research Center Jülich.

APPENDIX A: TRANSITION FREQUENCIES OF THE S-I_N SYSTEM AT HIGH FIELD

The transition frequencies of the S-I_N system can be extracted from the $2^{(N+1)}$ eigenvalues obtained by diagonalization of the Hamilton operator (1) in the Zeeman eigenbasis and by applying the selection rules at high field. An adequate set of quantum numbers at high field is given by the magnetic quantum number $m_S = \pm 1/2$ of the S spin, the total I spin $F_I \geqslant 0$, and the corresponding magnetic quantum number m_I, for which $-F_I \leqslant m_I \leqslant F_I$. The possible values for the total I spin are $F_I = (N/2) - k$ where $k = 0, 1, \ldots N/2$ for even N, and $k = 0, 1, \ldots (N-1)/2$ for odd N. Each energy level can be expressed as a function of F_I, m_I and m_S:

$$E(F_I, m_I, m_S) = (m_I + m_S)\,\nu_I - \frac{J}{4} + m_S \times \sqrt{(F_I + 1/2)^2 J^2 + 2J(m_I + m_S)(\nu_S - \nu_I) + (\nu_S - \nu_I)^2}. \tag{A1}$$

Equation (A1) is valid for arbitrary fields B. At high field we have $|\nu_S - \nu_I| \gg J$ and a Taylor expansion for the square root in Eq. (A1) up to second order in the small parameter $x = J/(\nu_I - \nu_S)$ leads to

$$E(F_I, m_I, m_S) = m_I \nu_I + m_S \nu_S + \left[m_S (m_I + m_S) - \frac{1}{4} \right] J + \frac{m_S}{2} [(F_I + 1/2)^2 - (m_I + m_S)^2] \frac{J^2}{\nu_S - \nu_I}. \tag{A2}$$

The transition frequencies of the I spin up to second order are determined by Eq. (A2) and by the I-spin selection rules at high field $\Delta m_I = \pm 1$, $\Delta m_S = 0$. This results in

$$E(F_I, m_I, m_S) - E(F_I, m_I - \Delta m_I, m_S) = \Delta m_I \nu_I + m_S \Delta m_I J + m_S \Delta m_I \times \frac{2(m_I + m_S) - \Delta m_I}{2} \frac{J^2}{\nu_I - \nu_S}. \tag{A3}$$

The transition frequencies of the S spin up to second order are determined by Eq. (A2) and by the S-spin selection rules

$\Delta m_S = \pm 1,\ \Delta m_I = 0$, giving

$$\begin{aligned} &E(F_I, m_I, m_S) - E(F_I, m_I, m_S - \Delta m_S) \\ &= \Delta m_S \nu_S + \Delta m_S (2m_S + m_I - \Delta m_S) J + \frac{\Delta m_S}{2} \\ &\quad \times \{ m_S [2(m_I + m_S) - \Delta m_S] - (F_I + 1/2)^2 \\ &\quad + (m_I + m_S - \Delta m_S)^2 \} \frac{J^2}{\nu_I - \nu_S}. \end{aligned} \tag{A4}$$

According to Eqs. (A3) and (A4), the transition frequencies of the S-I system up to second order are $\nu_{1,2} = \nu_S \mp J/2 - J^2/[4(\nu_I - \nu_S)]$ and $\nu_{3,4} = \nu_I \mp J/2 + J^2/[4(\nu_I - \nu_S)]$. They define two doublets at center frequency ν_S and ν_I both split by J. The second-order terms shift the doublet at center frequency ν_S by $-J^2/[4(\nu_I - \nu_S)]$ and the doublet at center frequency ν_I by $J^2/[4(\nu_I - \nu_S)]$.

The S-spin transition frequencies of the S-I_2 system at high field up to second order are given by $\nu_{1,4} = \nu_S \mp J - (1/2)J^2/(\nu_I - \nu_S)$, $\nu_2 = \nu_S - J^2/(\nu_I - \nu_S)$ and $\nu_3 = \nu_S$. These frequencies specify four transitions grouped around ν_S, where for $\nu_3 = \nu_S$ both I spins are in the singlet state and for the other three transitions the two I spins are in the triplet state. The I-spin transition frequencies are $\nu_{5,7} = \nu_I \mp J/2$ and $\nu_{6,8} = \nu_I \mp J/2 + (1/2)J^2/(\nu_I - \nu_S)$. The S-spin splitting $J^2/(\nu_I - \nu_S)$ between ν_2 and ν_3 is twice as large as for the I spin.

APPENDIX B: TRANSITION FREQUENCIES OF THE S-I_N SYSTEM AT LOW FIELD

The transition frequencies of the S-I_N group at low field can be obtained from Eq. (A1) and by introducing an appropriate set of quantum numbers. At low field $|\nu_I - \nu_S| \ll J$ so m_S and m_I are not good quantum numbers. The dominant quantum axis is defined by the J coupling between the S spin and all other I spins. So the good quantum numbers are the total spin $F = F_I + F_S$ [with $F_I = (N/2) - k$] and the corresponding magnetic quantum number $m_F = m_S + m_I$ with its possible values $-F \leqslant m_F \leqslant F$. For $F_I \neq 0$ the two possible values for the S spin with respect to the I spins are $F_S = \pm 1/2$. If $F_I = 0$ (singlet F state) $F_S = +1/2$ is single valued since the direction of the I spins relative to the S spin is not defined. From Eq. (A1) the possible energy levels can be expressed as a function of F_I, F_S and m_F:

$$\begin{aligned} E(F_I, F_S, m_F) &= m_F \nu_I - \frac{J}{4} + F_S \\ &\times \sqrt{(F_I + 1/2)^2 J^2 + 2 m_F J (\nu_S - \nu_I) + (\nu_S - \nu_I)^2}. \end{aligned} \tag{B1}$$

At low field we have $|\nu_I - \nu_S| \ll J$ and a Taylor expansion for the square root in Eq. (B1) up to second order in the small parameter $x = (\nu_S - \nu_I)/J$ leads to

$$\begin{aligned} &E(F_I, F_S, m_F) \\ &= \left[F_S (F_I + 1/2) - \frac{1}{4} \right] J + \left[1 - \frac{F_S}{F_I + 1/2} \right] m_F \nu_I \\ &\quad + \left[\frac{F_S}{F_I + 1/2} \right] m_F \nu_S + F_S \frac{(F_I + 1/2)^2 - m_F^2}{2(F_I + 1/2)^3} \frac{(\nu_S - \nu_I)^2}{J}. \end{aligned} \tag{B2}$$

The first term in Eq. (B2) is the energy of the J coupling at zero field, the second and third term describes the Zeeman splitting proportional to B, and the fourth term is a quadratic correction term in the B field. From the selection rules at low field for the 0 transitions (e.g., $\Delta F = 0$, $\Delta F_S = 0$, and $\Delta m_F = \pm 1$) the following 0 transition frequencies are obtained:

$$\begin{aligned} &E(F_I, F_S, m_F) - E(F_I, F_S, m_F - \Delta m_F) \\ &= \left[1 - \frac{F_S}{F_I + 1/2} \right] \nu_I + \left[\frac{F_S}{F_I + 1/2} \right] \nu_S \\ &\quad - F_S \frac{1 - 2\Delta m_F m_F}{2(F_I + 1/2)^3} \frac{(\nu_S - \nu_I)^2}{J}. \end{aligned} \tag{B3}$$

All transitions in Eq. (B3) for which $F_I + F_S = 0$ (singlet F state) is valid have to be excluded since there is no transition associated to a singlet state. From the selection rules for the J transitions (e.g., for $\Delta F = +1$, $\Delta F_S = +1$, $\Delta m_F = \pm 1$) we obtain the following J-transition frequencies:

$$\begin{aligned} &E(F_I, F_S, m_F) - E(F_I, F_S - 1, m_{F'} - \Delta m_F) \\ &= (F_I + 1/2) J + \left[\Delta m_F - \frac{F_S \cdot \Delta m_F + m_F - \Delta m_F}{F_I + 1/2} \right] \nu_I \\ &\quad + \left[\frac{F_S \Delta m_F + m_F - \Delta m_F}{F_I + 1/2} \right] \nu_S \\ &\quad + \frac{(F_I + 1/2)^2 - m_F^2 - (F_S - 1)(2\Delta m_F \cdot m_F - 1)}{2(F_I + 1/2)^3} \\ &\quad \times \frac{(\nu_S - \nu_I)^2}{J}. \end{aligned} \tag{B4}$$

Equation (B4) is defined only for $F_I > 0$. The linear combinations $(\alpha\gamma_I + \beta\gamma_S)B$, where α and β are identical with the two terms in the square brackets in Eqs. (B3) and (B4), define the new gyromagnetic ratios. For $\gamma_I \to \gamma_S$ only one transition in Eq. (B3) at frequency $\nu_I = \gamma_I \cdot B$ remains.

From Eqs. (B3) and (B4) the explicit expressions for the S-I system can be derived. The two 0 transitions are $\nu_{1,2} = (1/2)(\nu_I + \nu_S) \mp (\nu_I - \nu_S)^2/4J$ and the two J transitions are given by $\nu_{3,4} = J \mp (1/2)(\nu_I + \nu_S) + (\nu_I - \nu_S)^2/4J$. To first order ($B_1^{\text{low}} < B < B_2^{\text{low}}$) the S-I group has one zero transition at $\nu_1 = (1/2)(\nu_I + \nu_S)$ and two J transitions at frequencies $\nu_{2,3} = J \mp (1/2)(\nu_I + \nu_S)$ [Fig. 5(a)]. The five 0 transitions for the S-I_2 system to second order are given by $\nu_1 = \nu_S$, $\nu_{2,4} = (1/3)(2\nu_I + \nu_S) \mp 4(\nu_I - \nu_S)^2/27J$, $\nu_3 = (1/3)(2\nu_I + \nu_S)$, and $\nu_5 = (1/3)(4\nu_I - \nu_S)$. The corresponding four 3 $J/2$ transitions are given by $\nu_{6,9} = 3J/2 \mp \nu_I + 8(\nu_I - \nu_S)^2/27J$ and by $\nu_{7,8} = 3J/2 \mp (\nu_I/3 + 2\nu_S/3) + 4(\nu_I - \nu_S)^2/27J$. To first order the S-I_2transitions are reduced to three 0 transitions, $\nu_1 = \nu_S$, $\nu_2 = (1/3)(2\nu_I + \nu_S)$, and $\nu_3 = (1/3)(4\nu_I - \nu_S)$ and four 3 $J/2$ transitions at $\nu_{4,7} = 3J/2 \mp \nu_I$ and at $\nu_{5,6} = 3J/2 \mp (\nu_I/3 + 2\nu_S/3)$ [Fig. 5(b)].

APPENDIX C: PROOF OF THE MAXIMUM NUMBER OF LINES FOR THE S-I_N SYSTEM

We proof for odd N that the maximum number of lines for the S-I_N system is $(N+1)^2$. The proof for even N is

similar. Consider the two cases $N = 1, 3$ in Figs. 5(a) and 5(c). We can divide the states with total spin $F = F_I \pm 1/2$, with $F_I = (N/2) - k$ into spin states $F^+_{(k)} = F_I + 1/2 = (N+1)/2 - k$ $(k = 0, 1, \ldots (N+1)/2)$ with positive energy and into states $F^-_{(k)} = F_I - 1/2 = (N-1)/2 - k$ $(k = 0, 1, \ldots (N-1)/2)$ with negative energy. Each F state has $2F$ possible zero-frequency transitions so the total number of 0 transitions is

$$\begin{aligned}
&\sum_{k=0}^{(N+1)/2} 2F^+_{(k)} + \sum_{k=0}^{(N-1)/2} 2F^-_{(k)} \\
&\quad = \sum_{k=0}^{(N+1)/2} (N+1-2k) + \sum_{k=0}^{(N-1)/2} (N-1-2k) \\
&\quad = N+1-2[(N+1)/2] + \sum_{k=0}^{(N-1)/2} (2N-4k) \\
&\quad = 2\sum_{k=0}^{(N-1)/2} N-2k. \qquad \text{(C1)}
\end{aligned}$$

The total number of J transitions for odd N can be derived by inspection of Fig. 5. Obviously the number of possible transitions from each level $F^-_{(k)}$ is twice the total number of levels of the $F^-_{(k)}$ multiplets, so each $F^-_{(k)}$ multiplet is associated to $2(2F^-_{(k)} + 1)$ transitions. Therefore, the total number of J transitions is given:

$$\begin{aligned}
2\sum_{k=0}^{(N-1)/2} (2F^-_{(k)} + 1) &= 2\sum_{k=0}^{(N-1)/2} \{2[(N-1)/2 - k] + 1\} \\
&= 2\sum_{k=0}^{(N-1)/2} N - 2k. \qquad \text{(C2)}
\end{aligned}$$

The last expressions in Eqs. (C1) and (C2) involve the sum over the first $(N+1)/2$ odd numbers, which is identical to $[(N+1)/2]^2$. The total number of 0 and J transitions is given by the sum of Eqs. (C1) and (C2), which results in

$$4\sum_{k=0}^{(N-1)/2} N - 2k = 4\left(\frac{N+1}{2}\right)^2 = (N+1)^2. \qquad \text{(C3)}$$

This completes the proof for odd N. A similar proof holds for even N with the difference that the sum is taken over even numbers and that the total number of 0 transitions is higher by one than the total number of J transitions. Finally we note that all possible combination lines at high field (the flip (or flop) process of two I spins combined with the flop (or flip) process of one S spin [2]) transform at ultralow field to the sum of all possible 0 transitions of those multiplets with negative energy (see Fig. 5). Therefore the total number of combination lines for the S-I_N system is given by $\sum_{k=0}^{(N-1)/2} 2F^-_{(k)}$. For $N = 2$, 3, and 4 we have one, two, and four combination lines.

[1] R. R. Ernst, G. Bodenhausen, and A. Wokaun, *Principles of Nuclear Magnetic Resonance in One and Two Dimensions* (Clarendon Press, Oxford, 1987).

[2] H. Günther, *NMR Spectroscopy* (John Wiley & Sons, New York, 1973).

[3] J. T. Arnold, S. S. Dharmatti, and M. E. Packard, J. Chem. Phys. **19**, 507 (1951).

[4] W. G. Proctor and F. C. Yu, Phys. Rev. **77**, 717 (1950); **81**, 20 (1951).

[5] E. L. Hahn and D. E. Maxwell, Phys. Rev. **88**, 1070 (1952).

[6] H. S. Gutowsky, D. W. McCall, and C. P. Slichter, J. Chem. Phys. **21**, 279 (1953).

[7] P. L. Corio, Chem. Rev. **60**, 363 (1960).

[8] S. Appelt, G. Wäckerle, and M. Mehring, in *NMR and More*, *in Honour of Anatole Abragam*, edited by M. Goldman and M. Porneuf (Les Editions de Physique Les Ullis, 1994), pp. 31–45.

[9] T. E. Chupp and R. J. Hoare, Phys. Rev. Lett. **64**, 2261 (1990).

[10] D. B. Zax, A. Bielecki, K. W. Zilm, A. Pines, and D. P. Weitekamp, J. Chem. Phys. **83**, 4877 (1985).

[11] D. B. Zax, A. Bielecki, K. W. Zilm, and A. Pines, Chem. Phys. Lett. **106**, 550 (1984).

[12] V. S. Greshishkin, Appl. Phys. A **55**, 505 (1992).

[13] M. P. Ledbetter *et al.*, J. Magn. Reson. **199**, 25 (2009).

[14] J. Perlo *et al.*, Science **308**, 1279 (2005).

[15] J. Perlo, F. Casanova, and B. Blümich, Science **315**, 1110 (2007).

[16] B. Blümich, F. Casanova, and S. Appelt, Chem. Phys. Lett. **477**, 231 (2009).

[17] R. McDermott *et al.*, Science **295**, 2247 (2002).

[18] S. Appelt, F. W. Häsing, H. Kühn, J. Perlo, and B. Blümich, Phys. Rev. Lett. **94**, 197602 (2005).

[19] S. Appelt, H. Kühn, F. W. Häsing, and B. Blümich, Nat. Phys. **2**, 105 (2006).

[20] J. N. Robinson *et al.*, J. Magn. Reson. **182**, 343 (2006).

[21] I. M. Savukov and M. V. Romalis, Phys. Rev. Lett. **94**, 123001 (2005).

[22] S. Appelt, F. W. Häsing, H. Kühn, and B. Blümich, Phys. Rev. A **76**, 023420 (2007).

[23] S. Appelt, F. W. Häsing, H. Kühn, U. Sieling, and B. Blümich, Chem. Phys. Lett. **440**, 308 (2007).

[24] I. K. Kominis, T. W. Kornack, J. C. Allred, and M. V. Romalis, Nature **422**, 596 (2003).

[25] J. Clarke, in *SQUID Sensors: Fundamentals, Fabrication and Applications*, edited by H. Weinstock (Kluwer Academic, Dordrecht, 1996), pp. 1–62.

[26] Y. S. Greenberg, Rev. Mod. Phys. **70**, 175 (1998).

[27] M. E. Halse, P. T. Callaghan, B. C. Feland, and R. E. Wasylishen, J. Magn. Reson. **200**, 88 (2009).

[28] P. J. Hore, J. A. Jones, and S. Wimperis, *NMR: The Toolkit* (Oxford University Press, Oxford, 2000).

[29] M. A. Bouchiat, T. R. Carver, and C. M. Varnum, Phys. Rev. Lett. **5**, 373 (1960).

[30] W. Happer, Rev. Mod. Phys. **44**, 169 (1972).

[31] B. Driehuys *et al.*, Appl. Phys. Lett. **69**, 1668 (1996).
[32] S. Appelt, A. B. Baranga, C. J. Erickson, M. Romalis, A. R. Young, and W. Happer, Phys. Rev. A **58**, 1412 (1998).
[33] G. Navon *et al.*, Science **271**, 1848 (1996).
[34] C. R. Bowers and D. P. Weitekamp, Phys. Rev. Lett. **57**, 2645 (1986).
[35] M. Goldman, H. Jóhannesson, O. Axelsson, and M. Karlsson, Magn. Reson. Imaging **23**, 153 (2005).
[36] R. W. Adams, Science **323**, 1708 (2009).
[37] B. D. Armstrong *et al.*, J. Magn. Reson. **191**, 273 (2003).
[38] J. R. Maze *et al.*, Nature **455**, 644 (2008).
[39] S. Appelt *et al.*, Chem. Phys. Lett. **485**, 217 (2010).